Defect-Rich Heterogeneous MoS$_2$/NiS$_2$ Nanosheets Electrocatalysts for Efficient Overall Water Splitting

Jinghuang Lin, Pengcheng Wang, Haohan Wang, Chun Li, Xiaoqing Si, Junlei Qi,* Jian Cao, Zhengxiang Zhong, Weidong Fei, and Jicai Feng

Designing and constructing bifunctional electrocatalysts is vital for water splitting. Particularly, the rational interface engineering can effectively modify the active sites and promote the electronic transfer, leading to the improved splitting efficiency. Herein, free-standing and defect-rich heterogeneous MoS$_2$/NiS$_2$ nanosheets for overall water splitting are designed. The abundant heterogeneous interfaces in MoS$_2$/NiS$_2$ can not only provide rich electroactive sites but also facilitate the electron transfer, which further cooperate synergistically toward electrocatalytic reactions. Consequently, the optimal MoS$_2$/NiS$_2$ nanosheets show the enhanced electrocatalytic performances as bifunctional electrocatalysts for overall water splitting. This study may open up a new route for rationally constructing heterogeneous interfaces to maximize their electrochemical performances, which may help to accelerate the development of nonprecious electrocatalysts for overall water splitting.

The electrolysis of water offers a promising solution to produce clean and renewable hydrogen fuel supply.[1] Electrocatalytic water splitting involving two half reactions, hydrogen evolution reaction (HER) and oxygen evolution reaction (OER), requires highly efficient electrocatalysts such as Pt for HER and RuO$_2$ or IrO$_2$ for OER to lower the activation barrier and boost the reaction process.[2,3] However, the high cost and scarcity of

J. Lin, P. Wang, H. Wang, C. Li, X. Si, Prof. J. Qi
State Key Laboratory of Advanced Welding and Joining
Harbin Institute of Technology
Harbin 150001, China
E-mail: jlqi@hit.edu.cn
Prof. J. Cao, Prof. W. Fei, Prof. J. Feng
School of Materials Science and Engineering
Harbin Institute of Technology
Harbin 150001, China
Z. Zhong
MIIT Key Laboratory of Critical Materials Technology for New Energy
Conversion and Storage
State Key Laboratory of Urban Water Resource and Environment
School of Chemistry and Chemical Engineering
Harbin Institute of Technology
Harbin 150001, China

The ORCID identification number(s) for the author(s) of this article can be found under https://doi.org/10.1002/advs.201900246.

these noble electrocatalysts seriously limited their wide application.[4] In view of the above situation, tremendous effort has been devoted to develop nonprecious yet efficient catalysts for OER and HER simultaneously.[5,6]

Among these potential candidates, transition metal sulfides (TMSs), such as MoS$_2$, CoS$_2$, and NiS$_2$, have drawn extensive attention, due to their considerable electrocatalytic performances.[7,8] However, the limited electroactive sites and insufficient stability of these TMSs seriously restricted the improved electrocatalytic activity.[9,10] Element doping would be an effective method to improve the catalytic activities, such as doping Ni atoms in MoS$_2$.[1,7] Considering that surfaces or interfaces play the key role in electrochemical reactions, the morphology, surface defects or interfaces, and electrical structures are the key factors on the electrocatalytic performances of efficient catalysts.[11–15] As for tuning the morphology, constructing 2D TMS nanosheets could generate abundant electroactive sites because of inherent large specific surface and rich active edges.[16,17] In particular, in situ growing nanosheet nanostructures on conductive substrates, such as Ni foam, carbon cloth, and stainless steel, could supply the efficient pathways for charge transport and provide open channels for rapid release of gas bubbles during OER or HER process.[18–20] Further, interface modification could be another effective approach to engineering the physical or chemical properties of electrocatalysts.[21,22] The interface engineering could be beneficial to enrich the active sites and promote the electronic transfer, and thus boost the sluggish water splitting efficiency.[23,24] Additionally, owing to the different chemical reactivity, there are abundant interior defects in bimetal sulfide hybrids.[25,26] Undoubtedly, the defects in bimetal sulfide hybrids have a significant impact on electrical behavior, and thus modify the electrocatalytic performances.[25,26] Consequently, it is highly desirable to design and construct defected heterogeneous nanosheets with abundant electroactive sites directly on conductive substrates for overall water splitting.

Herein, we successfully construct defect-rich heterogeneous MoS$_2$/NiS$_2$ nanosheets directly on carbon cloth and investigate the influence of interface configuration on the electrocatalytic performances. The defect-rich interfaces with disordered structure are confirmed by the high-resolution transmission electron microscopy (HRTEM), and X-ray photoelectron spectroscopy
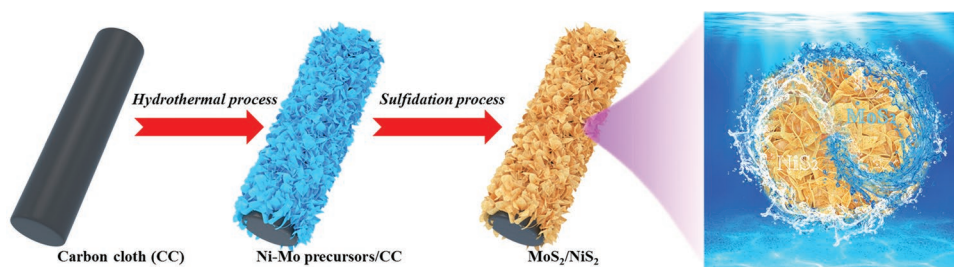
Figure 1. Schematic illustration for the formation of defect-rich heterogeneous MoS_2/NiS_2 nanosheets.

(XPS) further evidences the strengthened interfacial effects between MoS_2 and NiS_2. Consequently, the optimal MoS_2/NiS_2 nanosheets present low overpotentials of 62 and 278 mV at 10 mA cm^{-2} for HER and OER, respectively. Further, for overall water splitting, the optimal MoS_2/NiS_2 nanosheets exhibit a voltage of 1.59 V at 10 mA cm^{-2} as well as good stability.

The fabrication of defect-rich heterogeneous MoS_2/NiS_2 nanosheets involves two steps, as schematically shown in **Figure 1**. First, Ni-Mo precursors were synthesized on carbon cloth by the hydrothermal process. Second, MoS_2/NiS_2 nanosheets were synthesized by annealing the Ni-Mo precursors

with sublimed sulfur in Ar atmosphere at 400 °C for 1 h. And different MoS_2/NiS_2 nanosheets are prepared by finely controlling the amount of sublimed sulfur (50, 100, 200, and 400 mg), which is briefly named as MoS_2/NiS_2-1, 2, 3, and 4. For comparison, pure NiS_2 nanosheets also are prepared by the similar process and more detailed information could be found in Supporting Information. And pure $NiMoO_4$ nanosheets are also synthesized by annealing Ni-Mo precursors in air.

The crystal phases of obtained samples are investigated by X-ray diffraction (XRD) analysis, as shown in **Figure 2**a. Evidently, all diffraction peaks except for the peak of carbon cloth could
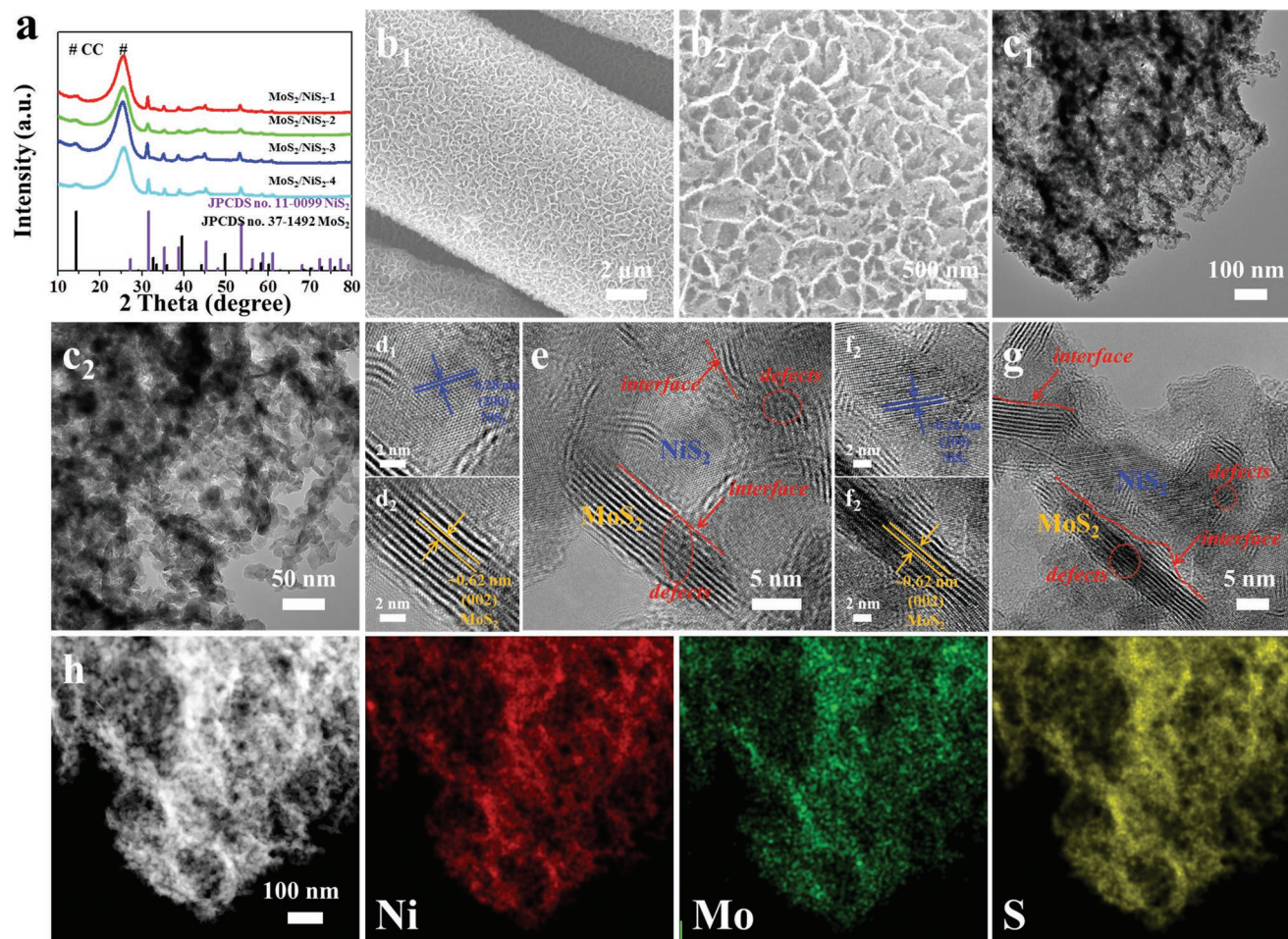

Figure 2. a) XRD patterns of obtained samples. b) SEM images of MoS_2/NiS_2-3 nanosheets. c–g) TEM and HRTEM images of MoS_2/NiS_2-3 nanosheets. h) The corresponding element mappings in MoS_2/NiS_2-3 nanosheets.
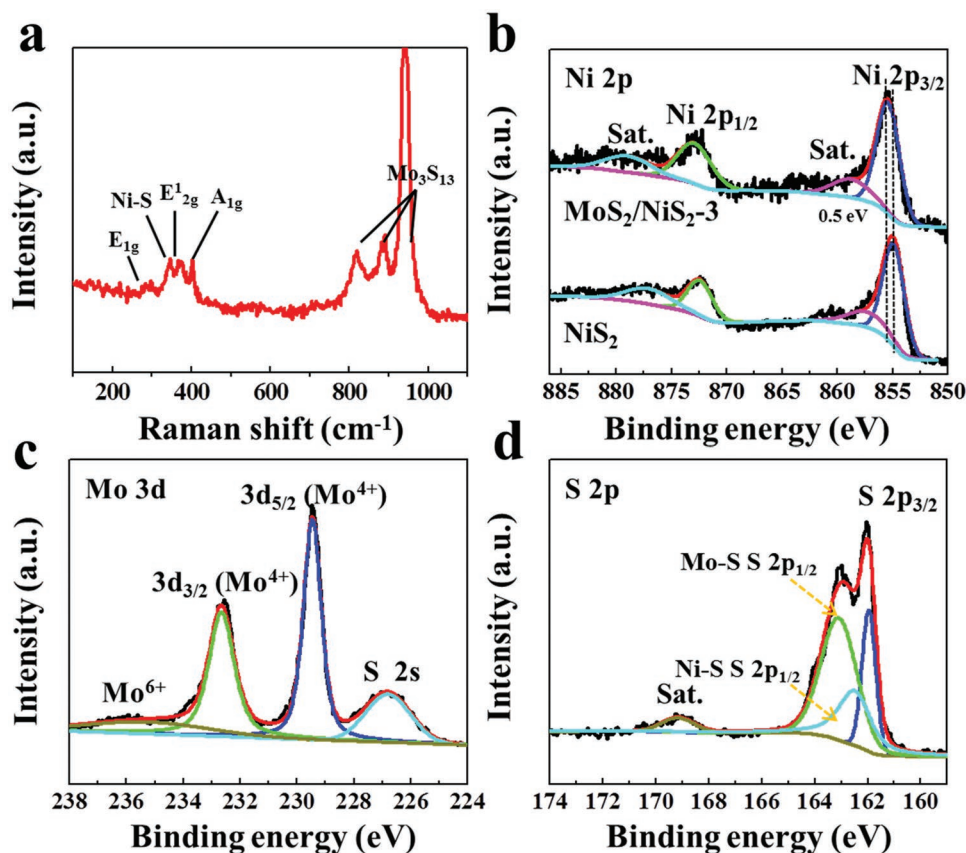
Figure 3. a) Raman spectrum of MoS$_2$/NiS$_2$-3 nanosheets. High-resolution XPS profiles of b) Ni 2p of MoS$_2$/NiS$_2$-3 and NiS$_2$, c) Mo 3d, and d) S 2p in MoS$_2$/NiS$_2$-3 nanosheets.

be well indexed to NiS$_2$ (Joint Committee on Powder Diffraction Standards (JCPDS) Card No. 11-0099)[6] and MoS$_2$ (JCPDS Card No. 37-1492),[12] suggesting the presence of metal sulfides. The morphologies of obtained samples are characterized by scanning electron microscopy (SEM), as shown in Figure 2b. A porous, discontinuous, and loose surface could be found in MoS$_2$/NiS$_2$-3, while a continuous and compact surface could be observed for MoS$_2$/NiS$_2$-1 (Figure S3a, Supporting Information). And with excessive sulfur source, the MoS$_2$/NiS$_2$-4 nanosheets have been seriously etched and more porous nanosheets could be formed (Figure S3d, Supporting Information). From the SEM images in Figure 2b and Figure S3 in the Supporting Information, it can be found that various morphologies and structures of MoS$_2$/NiS$_2$ nanosheets could be prepared by finely controlling the amount of sublimed sulfur. Again, the TEM images in Figure 2c confirm that MoS$_2$/NiS$_2$-3 nanosheets possess the amounts of nanoholes, which could provide more electroactive sites for catalytic reactions. The Brunauer–Emmett–Teller specific surface area of MoS$_2$/NiS$_2$-3 nanosheets was calculated as 56.6 m^2 g^{-1}, again suggesting the rich active sites for electrochemical reactions. In the HRTEM images (Figure 2d–g), the lattice fringe of 0.62 nm belong to the (002) lattice plane of MoS$_2$, while the lattice distances of 0.28 nm are indexed to (200) plane of NiS$_2$. More importantly, clear heterointerfaces derived from the mismatch of MoS$_2$ and NiS$_2$ in Figure 2e,g could result in rich defects and disordered structure. Such heterointerfaces

in obtained sulfides are beneficial for promoting HER performances, and it will be discussed in the following sections. Further, the energy dispersive X-ray spectroscopy mapping results (Figure 2h) show the homogeneously distribution of Ni, Mo, and S elements in MoS$_2$/NiS$_2$-3 nanosheets.

Since electrochemical reactions mainly occur on the surfaces or at the interfaces of electrocatalysts,[11–13] it is vital to investigate the surface states of obtained samples by Raman and XPS measurements. As shown in **Figure 3**a, the peaks at about 294, 375, and 404 cm^{-1} belong to E$_{1g}$, E$^1_{2g}$, and A$_{1g}$ modes of 2H-MoS$_2$, and the peak 345 cm^{-1} is from the modes of the Ni-S.[8,27–29] More importantly, the obvious three peaks in 800–1000 cm^{-1} could be ascribed to the molecular structure of Mo$_3$S$_{13}$ that existing the edge sites of MoS$_2$, and further suggest rich under-coordinated Mo-S edge sites in MoS$_2$/NiS$_2$-3 nanosheets.[8,28,29] As for Ni 2p in Figure 3b, two obvious peaks at 872.9 and 855.4 eV are attributed to the Ni 2p$_{1/2}$ and Ni 2p$_{3/2}$, as well two broad satellite peaks, demonstrating the presence of Ni^{2+}.[30] Compared to pure NiS$_2$, two peaks of Ni 2p$_{1/2}$ and Ni 2p$_{3/2}$ in MoS$_2$/NiS$_2$-3 are slightly shifted to higher binding energies (about 0.5 eV). It suggests the strong electronic interactions between NiS$_2$ and MoS$_2$ domains through established heterogeneous interfaces.[31,32] As for Mo 3d in Figure 3c, the peaks at about 232.4 and 229.1 eV are corresponded to Mo 3d$_{3/2}$ and Mo 3d$_{5/2}$, suggesting the presence Mo^{4+}.[8] And the nearby peak at about 226.2 eV from S 2s suggests the formation of Ni-S
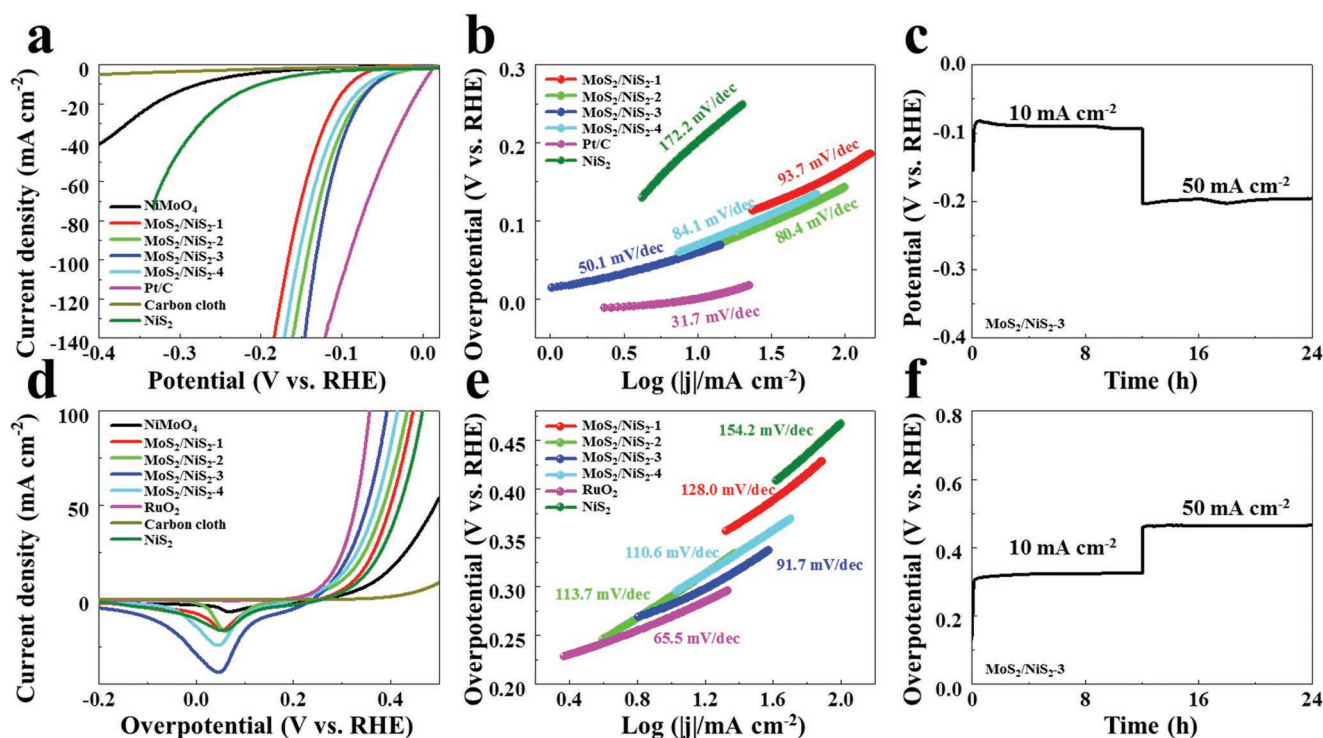
Figure 4. a) Polarization curves and b) the corresponding Tafel plots of obtained sample for HER. c) Chronopotentiometric curve of HER for MoS_2/NiS_2-3 nanosheets. d) Polarization curves and e) the corresponding Tafel plots of obtained sample for OER. f) Chronopotentiometric curve of OER for MoS_2/NiS_2-3 nanosheets.

and Mo-S bindings.[8,33] For S 2p spectra in obtained samples (Figure 3d), it can be deconvoluted into three peaks corresponding to the S $2p_{3/2}$, S $2p_{1/2}$ for Mo-S bond and S $2p_{1/2}$ for Ni-S bond, at as well as a peak from the oxidized species formed on the surface of metal sulfides.[3] The S $2p_{3/2}$ peak is attributed to the typical metal-S bond, while the S $2p_{1/2}$ corresponds to the sulfur with low coordination that is generally related to sulfur defects.[34,35] It suggests the presence of terminal unsaturated S atoms on Mo-S and Ni-S sites, which may be beneficial for HER performances.[35,36] Based on SEM, TEM, Raman, and XPS analysis, as-synthesized MoS_2/NiS_2 nanosheets are proved to possess porous nanostructure and defected interface for rich active sites and are expected to achieve excellent electrocatalytic performances.

The electrocatalytic HER and OER activities of heterogeneous MoS_2/NiS_2 nanosheets were measured in a three-electrode configuration using 1 M potassium hydroxide (KOH) as electrolyte. For comparison, the performance of the commercial Pt/C, RuO_2 and NiS_2 were also measured. **Figure 4**a presents the polarization curves of the samples with iR correction. As for MoS_2/NiS_2-3 nanosheets, the current density rapidly increases with the increased potential, demonstrating the remarkable HER performances. The MoS_2/NiS_2-3 nanosheets delivered an overpotential of 62, 108, and 131 mV at the current densities of 10, 50, and 100 mA cm^{-2}, superior to those of other counterparts, and comparable with Pt/C. As further compared with the current noble-metal-free catalysts (Table S1, Supporting Information), our MoS_2/NiS_2-3 nanosheets show the competitive electrocatalytic performances. When compared the HER performances of MoS_2/NiS_2 and pure NiS_2, the obvious improvement suggests

the synergy and mutual interaction between MoS_2 and NiS_2. In addition, we also prepared different samples by simply changing the annealing temperature, and the sublimed sulfur was fixed at 200 mg. As shown in Figures S6–S8 in the Supporting Information, MoS_2/NiS_2 obtained at 400 °C possesses the richest sulfur defects and shows the best HER and OER performances. These results demonstrate to some extent, sulfur defects could provide rich active sites and accelerate electron/mass transfer, resulting in improved catalytic performances.

To investigate the HER kinetic mechanism, the Tafel plots calculated from the polarization curves are shown in Figure 4b. The Tafel slop of MoS_2/NiS_2-3 nanosheets (50.1 mV dec^{-1}) is smaller than pure NiS_2 and other MoS_2/NiS_2 samples, while it is close to that of Pt/C (31.7 mV dec^{-1}). According to previous researches,[37,38] HER in KOH solution involves in three principal steps: i) Volmer reaction (Tafel slope of about 120 mV dec^{-1}), ii) Heyrovsky reaction (Tafel slope of about 40 mV dec^{-1}), and iii) Tafel reaction (Tafel slope of about 30 mV dec^{-1}). Such a Tafel slope of the MoS_2/NiS_2 nanosheet (50.1 mV dec^{-1}) suggests the HER reaction follows the Volmer–Heyrovsky mechanism ($H_2O + H_{ads} + e^- \rightarrow H_2 + OH^-$), where H_{ads} presents the H atom on an active site. Compared with pure NiS_2 (172.2 mV dec^{-1}), the obviously decreased Tafel slope of MoS_2/NiS_2-3 also confirms the enhanced Volmer step in HER kinetics.[8,30] From the XPS result in Figure 3b, it could be inferred that the electron density around Ni is reduced in MoS_2/NiS_2-3, which could provide sufficient empty d orbitals to improve the binding ability with H atoms.[31,39] Therefore, the improved H binding would facilitate the Volmer step, leading to the obviously decreased Tafel slope and enhanced HER

**ADVANCED
SCIENCE NEWS**

www.advancedsciencenews.com

**ADVANCED
SCIENCE**
Open Access

www.advancedscience.com

performances of MoS_2/NiS_2. Figure S9a shows the chrono-potentiometric curve for MoS_2/NiS_2-3 electrode at various current densities from 10 to 190 mA cm^{-2}. The potential shows no obvious changes in every step, indicating the good conductivity, excellent mass transport, and mechanical properties of MoS_2/NiS_2-3 electrode in HER tests. In the long-time stability test (Figure 4c), the MoS_2/NiS_2-3 electrode maintains a stable HER activity at different current densities ranging from 10 to 50 mA cm^{-2}. In addition, SEM and XRD results in Figure S10 in the Supporting Information demonstrate that the nanosheet structure and crystallinity of MoS_2/NiS_2-3 are well retained after the HER stability measurement. Consequently, the good HER performances could be attributed to the strengthened interfacial effects between MoS_2 and NiS_2 with multilevel interfaces. Further, the rich electroactive sites by structure fine tuning also make great contribution to the good HER performances.

Since OER is another key role for overall water splitting, the OER performances of these samples are further characterized. As shown in Figure 4d, the polarization curve of MoS_2/NiS_2-3 shows the remarkably improved OER activity with low overpotentials of 278, 352, and 393 mV at 10, 50, and 100 mA cm^{-2}. Further, the OER performances of MoS_2/NiS_2-3 are competitive among the current noble-metal-free catalysts (Table S2, Supporting Information). As shown in Figure 4e, the Tafel slope for MoS_2/NiS_2-3 is 91.7 mV dec^{-1}, which is lower than that of pure NiS_2 (154.2 mV dec^{-1}) and is close to that of RuO_2 (65.5 mV dec^{-1}). It indicates that the MoS_2/NiS_2-3 proceeds a faster OER kinetic.[40] The chronopotentiometric curve of MoS_2/NiS_2-3 electrode in Figure S9b in the Supporting Information shows no obvious changes in every step, suggesting the good conductivity, excellent mass transport, and mechanical properties in OER tests. Further, we also compared the electrochemical sensitive area by measuring the double-layer capacitance (C_{dl}) of these samples in Figure S9c in the Supporting Information. The C_{dl} of 6.32 mF cm^{-2} on MoS_2/NiS_2-3 is much higher than that of pure NiS_2 (2.70 mF cm^{-2}). Consequently, the higher C_{dl} value demonstrates the more efficient mass and charge transport capability on MoS_2/NiS_2-3 for OER.[41] Further, the Nyquist plots (Figure S9d, Supporting Information) show that the MoS_2/NiS_2-3 possesses the lowest transfer resistance, revealing the fastest electron transfer kinetics.[40,41] To investigate the stability for OER, a long-time chronopotentiometry measurement was carried out at 10 and 50 mA cm^{-2}. As shown in Figure 4f, no obvious degradation could be found, suggesting the good stability.

In order to get insight the reaction mechanism for OER, the MoS_2/NiS_2-3 after long-term OER tests was characterized by SEM, XRD, Raman, and XPS (Figure S12, Supporting Information). MoS_2/NiS_2-3 after long-term OER tests maintained the nanosheet morphology with a rougher and thicker surface, as shown in Figure S12a in the Supporting Information. XRD pattern in Figure S12b in the Supporting Information shows that the new phase of $Ni(OH)_2 \cdot 0.75H_2O$ is formed after OER. It suggests that the Mo content in MoS_2/NiS_2-3 is greatly reduced after long-term OER tests. The Raman result in Figure S12c in the Supporting Information also shows the 471 and 558 cm^{-1} peaks from the presence of NiOOH.[42] As for Ni 2p in Figure S12d in the Supporting Information, the energy separation of 17.6 eV demonstrate the presence of Ni^{3+}.[43,44]

In other word, it suggests that the surface Ni^{2+} was oxidized after continuous electrochemical tests. As in Figure S12e in the Supporting Information, the intensity of S 2p has been greatly reduced after OER stability tests, suggesting the loss of S element. And the intensity of Mo 3d (Figure S12f, Supporting Information) also suggests that Mo content is reduced after long-term OER tests. With respect to O 1s (Figure S12g, Supporting Information), the peaks at 530.4 and 532.3 eV correspond to the lattice oxygen and surface hydroxyls.[45] It suggests that nickel oxides/hydroxides are formed during OER process. According to previous researches,[45–49] metal sulfides could be formed corresponding oxides/hydroxides during OER process and the formed oxides/hydroxides are known as the electrocatalytically active phases.

To illustrate the effect of the interface between MoS_2 and NiS_2, we also we synthesized pure MoS_2 nanosheets on carbon cloth (see Figures S13 and S14, Supporting Information). Then, we scratched the MoS_2 and NiS_2 powders from the carbon cloth, then mechanically mixed MoS_2 and NiS_2 with the atomic ratio of Mo:Ni = 1:1 (denoted as MoS_2-NiS_2). The mechanically mixed MoS_2-NiS_2 powders were also prepared on carbon cloth for tests. As shown in Figure S15 in the Supporting Information, it can be found that MoS_2/NiS_2 shows much better HER and OER performances than that of mechanically mixed MoS_2-NiS_2 sample. And according to previous researches,[50,51] interface engineering could be beneficial to accelerate the HER and OER kinetics by modifying the chemisorption. Owing to the strong electronic interactions and synergistic effects, the formed interfaces between two active materials could reconstruct more active centers for catalytic reactions.[50,52,53] Consequently, these results further demonstrate the effect of the interface, which could enrich the active sites and promote the electronic transfer, and thus boost the sluggish water splitting efficiency.

Finally, the optimum MoS_2/NiS_2 was further used as bifunctional electrocatalyst for overall water splitting. As shown in **Figure 5**a, the device affords a current density of 10 mA cm^{-2} with a cell voltage of 1.59 V. As shown in Figure 5b, the measured voltage is slightly larger than calculated voltage in different current densities, which may be due to the difference in the testing system. As shown in Figure 5c, the low cell voltage (1.59 V at 10 mA cm^{-2}) for MoS_2/NiS_2 is competitive with recently reported bifunctional electrocatalysts, such as NiS-NiS$_2$ (1.58 V at 10 mA cm^{-2}),[54] Ni$_{0.33}$Co$_{0.67}$S$_2$‖NiCo$_2$O$_4$ (1.69 V at 10 mA cm^{-2}),[55] NiS-Ni$_2$P$_2$S$_6$ (1.64 V at 10 mA cm^{-2}),[56] MoS$_2$/NiS (1.64 V at 10 mA cm^{-2}),[52] MoS$_2$/NiS (1.61 V at 10 mA cm^{-2}),[57] NiS/Ni$_2$P (1.67 V at 10 mA cm^{-2}),[58] NiS/NiS$_2$ (1.62 V at 10 mA cm^{-2}),[59] Ni-Co-P (1.62 V at 10 mA cm^{-2}),[60] Co$_3$O$_4$@MoS$_2$ (1.59 V at 10 mA cm^{-2}),[61] and MoS$_2$-CoOOH (1.60 V at 10 mA cm^{-2}).[62] To investigate the faradaic efficiency, the amounts of H$_2$ and O$_2$ produced during water splitting were measured in Figure S16 in the Supporting Information. After comparing the measured and calculated gas amounts, the faradaic efficiency for MoS_2/NiS_2 is closed to 100%. Further, Figure 5d shows that MoS_2/NiS_2‖MoS_2/NiS_2 exhibits unnoticeable deterioration at 10 and 50 mA cm^{-2}, suggesting good stability during overall water splitting.

Overall, the improved OER and HER performances of as-synthesized MoS_2/NiS_2 nanosheets is attributed to following
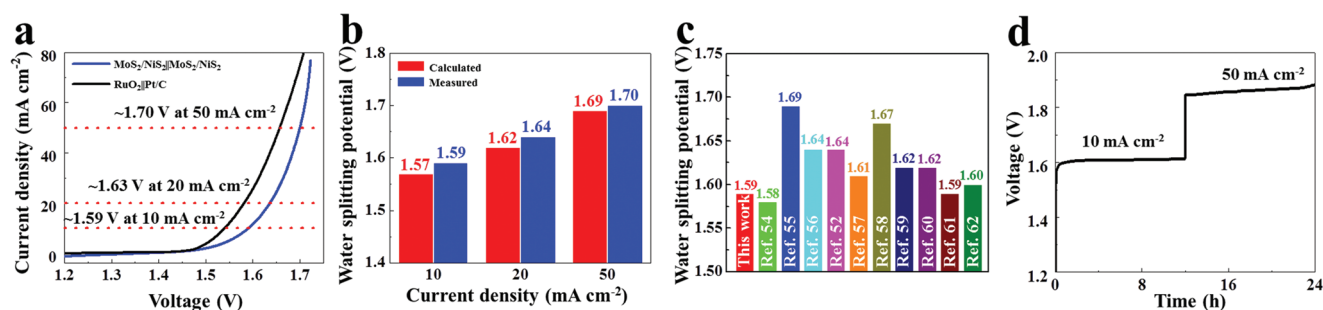
Figure 5. a) Polarization curves of optimal MoS_2/NiS_2 nanosheets and $RuO_2//Pt/C$ for overall water splitting. b) The comparison of calculated and measured water splitting potential. c) The comparison of overall water splitting performances between optimal MoS_2/NiS_2 nanosheets and other eletrocatalysts in reported literature. d) Chronopotentiometric curve of water electrolysis for optimal MoS_2/NiS_2 nanosheets.

aspects: 1) nanosheet arrays directly on carbon cloth could make sure the efficient pathways for charge transport and open channels for rapid release of gas bubbles. 2) The nanoholes by finely controlling the amount of sublimed sulfur could provide rich electroactive sites for catalytic reactions. 3) The strengthened interfacial effects between MoS_2 and NiS_2 could effectively modify the electronic interactions, contributing the electrocatalytic activities. 4) The abundant heterogeneous interfaces in MoS_2/NiS_2 could not only provide rich electroactive sites but also facilitate the electron transfer. Consequently, optimal MoS_2/NiS_2 nanosheets show the enhanced electrocatalytic performances for HER, OER, and overall water splitting.

In summary, free-standing and defect-rich heterogeneous MoS_2/NiS_2 nanosheets are successfully designed and fabricated, which serves as bifunctional electrocatalysts for overall water splitting. The derived MoS_2/NiS_2 interface with rich defects and disordered structure could modify the electronic interactions and facilitate the electron, which could be beneficial for electrocatalytic reactions. Further, the binder-free nanosheet arrays with rich nanoholes could also boost the HER and OER performances by providing rich electroactive sites and favoring the gas release from nanosheets. Consequently, working as both cathode and anode electrodes, the optimal MoS_2/NiS_2 nanosheets exhibit a voltage of 1.59 V at the current density of 10 mA cm^{-2}, as well as good stability. Therefore, rational construct and comprehension of heterogeneous interfaces offer a promising alternative to nonprecious electrocatalysts for overall water splitting.

Supporting Information

Supporting Information is available from the Wiley Online Library or from the author.

Acknowledgements

Conflict of Interest

The authors declare no conflict of interest.

Keywords

[1] Y. Huang, Y. Sun, X. Zheng, T. Aoki, B. Pattengale, J. Huang, X. He, W. Bian, S. Younan, N. Williams, J. Hu, J. Ge, N. Pu, X. Yan, X. Pan, L. Zhang, Y. Wei, J. Gu, *Nat. Commun.* **2019**, *10*, 982.
[2] Y. Luo, L. Tang, U. Khan, Q. Yu, H. Cheng, X. Zou, B. Liu, *Nat. Commun.* **2019**, *10*, 269.
[3] F. Li, D. Zhang, R. Xu, W. Fu, X. Lv, *ACS Appl. Energy Mater.* **2018**, *1*, 3929.
[4] H. Zhang, X. Li, A. Hähnel, V. Naumann, C. Lin, S. Azimi, S. L. Schweizer, A. W. Maijenburg, R. B. Wehrspohn, *Adv. Funct. Mater.* **2018**, *28*, 1706847.
[5] K. Xu, Y. Sun, Y. Sun, Y. Zhang, G. Jia, Q. Zhang, L. Gu, S. Li, Y. Li, H. J. Fan, *ACS Energy Lett.* **2018**, *3*, 2750.
[6] Y. Zhang, F. Lu, L. Pan, Y. Xu, Y. Yang, Y. Bando, D. Golberg, J. Yao, X. Wang, *J. Mater. Chem. A* **2018**, *6*, 11978.
[7] H. Zhang, L. Yu, T. Chen, W. Zhou, X. W. Lou, *Adv. Funct. Mater.* **2018**, *28*, 1807086.
[8] J. Staszak-Jirkovský, C. D. Malliakas, P. P. Lopes, N. Danilovic, S. S. Kota, K. Chang, B. Genorio, D. Strmcnik, V. R. Stamenkovic, M. G. Kanatzidis, N. M. Markovic, *Nat. Mater.* **2016**, *15*, 197.
[9] Y. Liu, C. Xiao, P. Huang, M. Cheng, Y. Xie, *Chem* **2018**, *4*, 1263.
[10] X. Y. Yu, X. W. Lou, *Adv. Energy Mater.* **2018**, *8*, 1701592.
[11] Y. P. Zhu, T. Y. Ma, M. Jaroniec, S. Z. Qiao, *Angew. Chem., Int. Ed.* **2017**, *56*, 1324.
[12] S. Liu, Y. Yin, M. Wu, K. S. Hui, K. N. Hui, C. Ouyang, S. C. Jun, *Small* **2019**, *15*, 1803984.
[13] S. Ye, Z. Shi, J. Feng, Y. Tong, G. Li, *Angew. Chem., Int. Ed.* **2018**, *57*, 2672.
[14] J. Feng, J. Wu, Y. Tong, G. Li, *J. Am. Chem. Soc.* **2018**, *140*, 5118.
[15] K. N. Dinh, X. Sun, Z. Dai, Y. Zheng, P. Zheng, J. Yang, J. Xu, Z. Wang, Q. Yan, *Nano Energy* **2018**, *54*, 82.
[16] G. Zhang, Y. Feng, W. Lu, D. He, C. Wang, Y. Li, X. Wang, F. Cao, *ACS Catal.* **2018**, *8*, 5431.
[17] M. S. Islam, M. Kim, X. Jin, S. M. Oh, N. Lee, H. Kim, S. Hwang, *ACS Energy Lett.* **2018**, *3*, 952.
[18] B. Liu, Y. Wang, H. Peng, R. Yang, Z. Jiang, X. Zhou, C. Lee, H. Zhao, W. Zhang, *Adv. Mater.* **2018**, *30*, 1803144.
[19] D. Wang, Q. Li, C. Han, Z. Xing, X. Yang, *ACS Cent. Sci.* **2018**, *4*, 112.

[20] S. Deng, Y. Zhong, Y. Zeng, Y. Wang, X. Wang, X. Lu, X. Xia, J. Tu, *Adv. Sci.* **2018**, *5*, 1700772.

[21] H. Ding, Q. Jiao, H. Lv, K. Xu, Q. Xing, M. Chen, W. Chu, X. Wu, Y. Guo, *J. Mater. Chem. A* **2018**, *6*, 17488.

[22] Y. Li, J. Yin, L. An, M. Lu, K. Sun, Y. Zhao, D. Gao, F. Cheng, P. Xi, *Small* **2018**, *14*, 1801070.

[23] C. Guo, Y. Zheng, J. Ran, F. Xie, M. Jaroniec, S. Qiao, *Angew. Chem., Int. Ed.* **2017**, *56*, 8539.

[24] Z. Zhang, X. Ma, J. Tang, *J. Mater. Chem. A* **2018**, *6*, 12361.

[25] J. Zhang, W. Xiao, P. Xi, S. Xi, Y. Du, D. Gao, J. Ding, *ACS Energy Lett.* **2017**, *2*, 1022.

[26] C. Zhang, Y. Shi, Y. Yu, Y. Du, B. Zhang, *ACS Catal.* **2018**, *8*, 8077.

[27] M. A. R. Anjum, H. Y. Jeong, M. H. Lee, H. S. Shin, J. S. Lee, *Adv. Mater.* **2018**, *30*, 1707105.

[28] J. Kibsgaard, T. F. Jaramillo, F. Besenbacher, *Nat. Chem.* **2014**, *6*, 248.

[29] D. Kong, Y. Wang, Y. V. Lim, S. Huang, J. Zhang, B. Liu, T. Chen, H. Y. Yang, *Nano Energy* **2018**, *49*, 460.

[30] G. F. Chen, T. Y. Ma, Z. Q. Liu, N. Li, Y. Z. Su, K. Davey, S. Z. Qiao, *Adv. Funct. Mater.* **2016**, *26*, 3314.

[31] Y. Yang, K. Zhang, H. Lin, X. Li, H. C. Chan, L. Yang, Q. Gao, *ACS Catal.* **2017**, *7*, 2357.

[32] L. An, J. Feng, Y. Zhang, R. Wang, H. Liu, G. Wang, F. Cheng, P. Xi, *Adv. Funct. Mater.* **2019**, *29*, 1805298.

[33] X. Wang, J. Wang, X. Sun, S. Wei, L. Cui, W. Yang, J. Liu, *Nano Res.* **2018**, *11*, 988.

[34] M. R. Gao, J. X. Liang, Y. R. Zheng, Y. F. Xu, J. Jiang, Q. Gao, J. Li, S. H. Yu, *Nat. Commun.* **2015**, *6*, 5982.

[35] Y. Li, K. Yin, L. Wang, X. Lu, Y. Zhang, Y. Liu, D. Yan, Y. Song, S. Luo, *Appl. Catal., B* **2018**, *239*, 537.

[36] J. Zhang, C. Zhang, Z. Wang, J. Zhu, Z. Wen, X. Zhao, X. Zhang, J. Xu, Z. Lu, *Small* **2018**, *14*, 1703098.

[37] Y. Zhu, G. Chen, Y. Zhong, W. Zhou, Z. Shao, *Adv. Sci.* **2018**, *5*, 1700603.

[38] Y. Zheng, Y. Jiao, Y. Zhu, L. H. Li, Y. Han, Y. Chen, A. Du, M. Jaroniec, S. Z. Qiao, *Nat. Commun.* **2014**, *5*, 3783.

[39] J. Greeley, T. F. Jaramillo, J. Bonde, I. B. Chorkendorff, J. K. Norskov, *Nat. Mater.* **2006**, *5*, 909.

[40] S. Dutta, A. Indra, Y. Feng, H. Han, T. Song, *Appl. Catal., B* **2019**, *241*, 521.

[41] Q. Xu, H. Jiang, H. Zhang, Y. Hu, C. Li, *Appl. Catal., B* **2019**, *242*, 60.

[42] Y. Li, H. Zhang, M. Jiang, Y. Kuang, X. Sun, X. Duan, *Nano Res.* **2016**, *9*, 2251.

[43] L. Hou, Y. Shi, C. Wu, Y. Zhang, Y. Ma, X. Sun, J. Sun, X. Zhang, C. Yuan, *Adv. Funct. Mater.* **2018**, *28*, 1705921.

[44] J. Lin, H. Wang, Y. Yan, X. Zheng, H. Jia, J. Qi, J. Cao, J. Tu, W. Fei, J. Feng, *J. Mater. Chem. A* **2018**, *6*, 19151.

[45] M. Lee, H. Oh, M. K. Cho, J. Ahn, Y. J. Hwang, B. K. Min, *Appl. Catal., B* **2018**, *233*, 130.

[46] O. Mabayoje, A. Shoola, B. R. Wygant, C. B. Mullins, *ACS Energy Lett.* **2016**, *1*, 195.

[47] R. Eadha, Y. R. Kumar, M. Sakar, K. R. Vinod, S. Balakumar, *Appl. Catal., B* **2018**, *225*, 386.

[48] B. Ni, T. He, J. Wang, S. Zhang, C. Ouyang, Y. Long, J. Zhuang, X. Wang, *Chem. Sci.* **2018**, *9*, 2762.

[49] F. Hu, S. Zhu, S. Chen, Y. Li, L. Ma, T. Wu, Y. Zhang, C. Wang, C. Liu, X. Yang, L. Song, X. Yang, Y. Xiong, *Adv. Mater.* **2017**, *29*, 1606570.

[50] J. Zhang, Q. Zhang, X. Feng, *Adv. Mater.* **2019**, 1808167.

[51] Z. W. Seh, J. Kibsgaard, C. F. Dickens, I. Chorkendorff, J. K. Nørskov, T. F. Jaramillo, *Science* **2017**, *355*, eaad4998.

[52] Q. Qin, L. Chen, T. Wei, X. Liu, *Small* **2018**, 1803639.

[53] R. Subbaraman, D. Tripkovic, K.-C. Chang, D. Strmcnik, A. P. Paulikas, P. Hirunsit, M. Chan, J. Greeley, V. Stamenkovic, N. M. Markovic, *Nat. Mater.* **2012**, *11*, 550.

[54] P. Luo, H. Zhang, L. Liu, Y. Zhang, J. Deng, C. Xu, N. Hu, Y. Wang, *ACS Appl. Mater. Interfaces* **2017**, *9*, 2500.

[55] Z. Peng, D. Jia, A. M. Al-Enizi, A. A. Elzatahry, G. Zheng, *Adv. Energy Mater.* **2015**, *5*, 1402031.

[56] X. Zhang, S. Zhang, J. Li, E. Wang, *J. Mater. Chem. A* **2017**, *5*, 22131.

[57] Z. Zhai, C. Li, L. Zhang, H. Wu, L. Zhang, N. Tang, W. Wang, J. Gong, *J. Mater. Chem. A* **2018**, *6*, 9833.

[58] X. Xiao, D. Huang, Y. Fu, M. Wen, X. Jiang, X. Lv, M. Li, L. Gao, S. Liu, M. Wang, C. Zhao, Y. Shen, *ACS Appl. Mater. Interfaces* **2018**, *10*, 4689.

[59] Q. Li, D. Wang, C. Han, X. Ma, Q. Lu, Z. Xing, X. Yang, *J. Mater. Chem. A* **2018**, *6*, 8233.

[60] E. Hu, Y. Feng, J. Nai, D. Zhao, Y. Hu, X. W. Lou, *Energy Environ. Sci.* **2018**, *11*, 872.

[61] J. Liu, J. Wang, B. Zhang, Y. Ruan, H. Wan, X. Ji, K. Xu, D. Zha, L. Miao, J. Jiang, *J. Mater. Chem. A* **2018**, *6*, 2067.

[62] B. Shang, P. Ma, J. Fan, L. Jiao, Z. Liu, Z. Zhang, N. Chen, Z. Cheng, X. Cui, W. Zheng, *Nanoscale* **2018**, *10*, 12330.

1900246 (7 of 7)